Iranian Journal of Science (2024) 48:479–486
https://doi.org/10.1007/s40995-024-01602-2

RESEARCH PAPER

Analysis of Gruneisen Parameter for Carbides and Bromides in Cast Iron

Shivam Srivastava[1] · Prachi Singh[1] · Anjani K. Pandey[2] · Chandra K. Dixit[1]

Received: 28 October 2023 / Accepted: 31 January 2024 / Published online: 15 March 2024

Abstract
In this current study, we delve into a comparative analysis of the Gruneisen parameter within the context of carbides and bromides embedded in cast iron under high compressive conditions. Our investigation is accompanied by a meticulous evaluation, wherein we juxtapose the outcomes with those derived from four distinct equations of states (EOSs): namely the M-L Jones EOS, Brennan–Stacey EOS, Birch–Murnaghan EOS, and Vinet–Rydberg EOS. Across the compression spectrum ranging from 1 to 0.91, our study unravels intriguing patterns. Notably, the modified Lenard Jones EOS emerges as the most fitting candidate for encapsulating the thermo elastic characteristics of carbides and bromides within the cast iron matrix. This assertion is substantiated by a distinctive observation: The modified Lenard Jones EOS yields a minimal slope in the graph depicting the relationship between the Gruneisen parameter and the volume compression ratio. In essence, our work sheds light on a compelling EOS choice, furthering our understanding of these materials' intricate behavior under extreme compression.

Keywords Cast iron · High pressure · Gruneisen parameter

1 Introduction

The intricate world of cast iron unveils an arsenal of mechanical marvels, where the interplay between composition, microstructure, and production methods crafts materials that withstand the harshest of environments. These alloys, recognized for their exceptional abrasive resistance, harbor secrets within their crystalline structures—secrets that hold the key to their remarkable mechanical prowess (Moustafa et al. 2000).

Within the heart of cast iron, concealed carbides and borides emerge as the unsung heroes, wielding the power to transform mundane iron into a formidable defender against wear and tear. These precipitated entities—Fe_2C, Fe_3C, $Fe_{23}C_7$, and their kin—bestow resilience upon the alloy. Yet, innovation has not ceased with tradition; a subtle infusion of chromium and boron, alchemical touchstones, reshapes these entities into (Fe, Cr)xC(B) formations (Feng et al. 2012). The outcome is a symphony of enhanced elasticity and tenacity, elevating the performance of these alloys above their ordinary counterparts. Unveiling the mystique behind this transformative alchemy requires more than just a discerning eye; it demands the precision of first principles calculations, grounded in the density functional theory (DFT).

This computational crucible illuminates the electronic tapestry, stability, and mechanical aptitude of these elusive compounds. As the veil of synthesis constraints lifts, ab initio calculations become the catalyst, enabling us to peer into the properties that define these alloys' mettle. The symphony of cast iron's mechanical performance echoes

✉ Shivam Srivastava
ss_phyphd2021@dsmnru.ac.in

Prachi Singh
psc_phyphd2021@dsmnru.ac.in

Anjani K. Pandey
anjani_phys@yahoo.in

Chandra K. Dixit
ckdixit@dsmnru.ac.in

[1] Department of Physics, Dr. Shakuntala Misra National Rehabilitation University, Lucknow, Uttar Pradesh, India

[2] Institute of Engineering and Technology, Dr. Shakuntala Misra National Rehabilitation University, Lucknow, Uttar Pradesh, India

across the realm of abrasion-resistant applications. This hinged harmony pivots on the trinity of chemical composition, micro structural nuances, and crafting techniques. Fracture toughness and hardness—essential attributes—find their roots entwined with the crystalline choreography of carbides and borides (Uhlenhaut et al. 2006; Zhou et al. 2009a; Shein et al. 2006; Xie et al. 2005). Their intricate crystal structures may stand before us, but the underlying physical and chemical nuances, shrouded by fabrication limitations, persist as enigmas. In the realm of understanding, scientific pioneers have ventured forth. Shein's voyage into the electronic and magnetic domains of X3C (where X dances with Fe, Co, Ni) unearthed the metastability of Fe3C and the allure of formation enthalpy. Meanwhile, Chen and colleagues, wielding empirical potentials, deciphered the stability and thermodynamics of X7C3 (Mn, Cr, Fe), while Music delved into Cr7C3's electronic tapestry. Fe2B, a polymorph of intrigue, unveiled its unstable visage through nonequilibrium sorcery (Music et al. 2004).

Such revelations expanded further—multi-component carbides (Fe, Si)3C, (Fe, Cr)3C, $Fe_{12}Cr_{12}W_4C_8B_4$—courted exploration. Si's dalliance with Fe_3C showcased solubility limitations, diverging from the script penned by Cr-doped Fe_3C. These crystalline serenades played out under the watchful gaze of first principles calculations. In this ongoing odyssey, Xiao, and peers ventured into the mechanical choreography of X2B compounds, their insights intertwining with the grand tapestry of knowledge. And now, in this narrative, we embark upon a similar voyage, where EOSs calculations unveil the intricate dances of carbides and borides within cast iron's realm. The mechanical properties of cast iron should consider the nano particle additive, which can greatly enhance the mechanical properties. (Xiao et al. 2011, 2010; Zhou et al. 2009b; Jang et al. 2009; Zuo and Liu 2021; Dixit et al. 2024).

The present study provided a different approach from convention existing models and the present approach is also shedding light on applicability of Equations of states. Various researchers have calculated the Gruneisen parameter from different equations of states, some of them have mentioned in the section of method of analysis. All the formulations of Gruneisen parameter have their own importance because they are applicable to various classes of materials (Srivastava et al. 2023b, c, g; Pandey et al. 2023a). Any single formulation of Gruneisen parameter cannot guarantee to be applicable on all class of materials even at high pressure range. So it become important to separate a good formulation of Gruneisen parameter from number of formulation existing, the present study provided such facility to the researchers. Various fundamental formulations to calculate Gruneisen parameter are given below…..

Slater gamma (Slater 1939) gave the formula for calculation of Gruneisen parameter which is given below……

$$\gamma = 0.5\left\{\frac{dK}{dP}\right\} - \left(\frac{1}{6}\right)$$

Vashchenko and Zubarev derived free volume expansion for Gruneisen parameter (Srivastava et al. 2023f).

$$\gamma = \frac{0.5\left\{\frac{dK}{dP}\right\} - \frac{5}{6} + \frac{2}{9}\left(\frac{P}{K_T}\right)}{1 - \left(\frac{4}{3}\right)\left(\frac{P}{K_T}\right)}$$

Borton and Stacey (Barton and Stacey 1985) gave the fallowing formula to calculate Gruneisen parameter…

$$\gamma = \frac{0.5\left\{\frac{dK}{dP}\right\} - \frac{1}{6} + \frac{2.35}{3}\left(1 - \frac{P}{3K_T}\right)}{1 - \left(\frac{4}{3}\right)\left(\frac{P}{K_T}\right)}$$

2 Method of Analysis

As the general form of straight line equation is $y = mx + c$, where m is slope of straight line from x axis. In the present analysis we have analyzed the Gruneisen parameter γ at high compression, so it is best suitable for us to replace y to γ and x to (V/V_0).

Now the equation of straight line becomes

$$\gamma = m\left(\frac{V}{V_0}\right) + c \tag{1}$$

Since the graph of Gruneisen parameter to V/V_0 is straight line and it passes through number of compression points. Taking only extreme points under consideration we will be able to analyze the slope of plots. Let at compression point $\left(\frac{V}{V_0}\right)_1$ the value of Gruneisen parameter is γ_1. While at compression point $\left(\frac{V}{V_0}\right)_2$ the value of Gruneisen parameter is γ_2.

Since all these points are within straight line so they will satisfy the equation of straight line.

From this we have obtained two different equation given fallowing.

$$\gamma_1 = m\left(\frac{V}{V_0}\right)_1 + c \tag{2}$$

and

$$\gamma_2 = m\left(\frac{V}{V_0}\right)_2 + c \tag{3}$$

From these two equations, we can easily obtain the value of slope of plot for Gruneisen parameter which is given by

$$m = \left[\frac{d\gamma}{d\left(\frac{V}{V_0}\right)}\right] = \left[\frac{\gamma_2 - \gamma_1}{\left(\frac{V}{V_0}\right)_2 - \left(\frac{V}{V_0}\right)_1}\right] \quad (4)$$

The EOS having minimum value of m will be the best suitable EOS for describing the thermo elastic properties of materials under consideration. For describing Gruneisen parameter we can obtain a straight line equation for it from Eqs. (1) and (2)

$$\gamma = \gamma_1 + m\left[\left(\frac{V}{V_0}\right) - \left(\frac{V}{V_0}\right)_1\right] \quad (5)$$

Now from Eqs. (4) and (5) we will obtain fallowing relationship.

$$\gamma = \gamma_1 + \left[\frac{\gamma_2 - \gamma_1}{\left(\frac{V}{V_0}\right)_2 - \left(\frac{V}{V_0}\right)_1}\right]\left[\left(\frac{V}{V_0}\right) - \left(\frac{V}{V_0}\right)_1\right] \quad (6)$$

The Equations of states developed by Brennan–Stacey, Vinet–Rydberg, Birch–Murnaghan, and modified Lenard Jones are given below, respectively, by Eqs. (7–10)……..

$$P = \frac{3K_0x^{-4}}{(3K_0\prime - 5)}\left[\exp\left\{\frac{(3K_0\prime - 5)(1 - x^3)}{3}\right\} - 1\right] \quad (7)$$

$$P = 3K_0x^{-2}(1 - x)\exp[\eta(1 - x)] \quad (8)$$

$$P = \frac{3}{2}K_0[x^{-7} - x^{-5}][1 + \frac{3}{4}(K_0\prime - 4)(x^{-2} - 4)] \quad (9)$$

where $x = \left(\frac{V}{V_0}\right)^{\frac{1}{3}}$ and $\eta = \frac{3}{2}(K'_0 - 1)$

$$P = \left(\frac{K_0}{n}\right)(y)^{-n}[y^{-n} - 1] \quad (10)$$

where $n = \frac{K_0\prime}{3}$ and $y = \left(\frac{V}{V_0}\right)$.

3 Results and Discussion

The important input parameters used in the analysis of Gruneisen parameter are given in the Table 1:

The values of Gruneisen parameter obtained from different EOS are illustrated in the Figs. 1, 2, 3 and 4. The formulation predicted by Borton and Stacey (Barton and Stacey 1985) for Gruneisen parameter have been used in the analysis of carbides and bromides in cast irons. Four different EOSs viz. modified Lenard Jones (Sun 2005), Brennan–Stacey (Stacey et al. 1981; Pandey et al. 2023b), Vinet–Rydberg (Vinet et al. 1986; Pandey et al. 2023c), and Birch–Murnaghan EOS (Birch 1947; Pandey et al. 2023e; Srivastava et al. 2023a) have been used. The values of pressure and Gruneisen parameter at high compression

Table 1 Table for Bulk modulus and pressure derivative of bulk modulus at zero pressure

Species	K_0(GPa)	$K_0\prime$	References
$Fe_{12}Cr_{12}W_4C_{12}$	358.56	5.81	Feng et al. (2012)
Fe_2B	331.04	4.44	Feng et al. (2012)
Fe_3C	259.20	4.25	Feng et al. (2012)
$Fe_{12}Cr_{12}W_4C_8B_4$	306.64	4.29	Feng et al. (2012)

obtained from different EOS are given in Tables 2, 3, 4, and 5.

From Fig. 1 and Table 4, we can observe that the modified Lenard Jones EOS has minimum slope while Vinet–Rydberg EOS has maximum slope. For calculation of slope of plots we can use Eq. (4)

$$\text{Slope } \frac{d\gamma}{d\left(\frac{V}{V_0}\right)} = \left[\frac{\gamma_2 - \gamma_1}{\left(\frac{V}{V_0}\right)_2 - \left(\frac{V}{V_0}\right)_1}\right].$$

So the slope for modified Lenard Jones EOS is $\left[\frac{d\gamma}{d\left(\frac{V}{V_0}\right)}\right]_{M-L\ \text{Jones}} = \frac{1.882657 - 1.995}{0.91 - 1} = 0.80381.$

and the slope for Vinet–Rydberg EOS is $\left[\frac{d\gamma}{d\left(\frac{V}{V_0}\right)}\right]_{\text{Brennan}-\text{StaceyEOS}} = \frac{1.747357 - 1.955}{0.91 - 1} = 2.307.$

So from these calculations we can observe that the graph of Gruneisen parameter obtained from modified Lenard Jones EOS makes an angle 38.79° while an angle of 66° formed in case of Vinet–Rydberg EOS from (V/V_0) axis. So from these observations we can see that the values obtained from modified Lenard Jones EOS are decreasing but very slowly in comparison with other. The modified Lenard Jones EOS is useful to calculate Gruneisen parameter up to compression range 0.91 for $Fe_{12}Cr_{12}W_4C_{12}$.

$$\text{Slope } \frac{d\gamma}{d\left(\frac{V}{V_0}\right)} = \left[\frac{\gamma_2 - \gamma_1}{\left(\frac{V}{V_0}\right)_2 - \left(\frac{V}{V_0}\right)_1}\right].$$

So the slope for modified Lenard Jones EOS is $\left[\frac{d\gamma}{d\left(\frac{V}{V_0}\right)}\right]_{M-L\ \text{Jones}} = \frac{1.249495 - 1.27}{0.91 - 1} = 0.227833.$

and the slope for Brennan–Stacey EOS is $\left[\frac{d\gamma}{d\left(\frac{V}{V_0}\right)}\right]_{\text{Brennan}-\text{StaceyEOS}} = \frac{1.134989 - 1.27}{0.91 - 1} = 1.5$

The above mathematical analysis explains distinct characteristics among different equations of states (EOS), while calculating the slopes derived from calculations

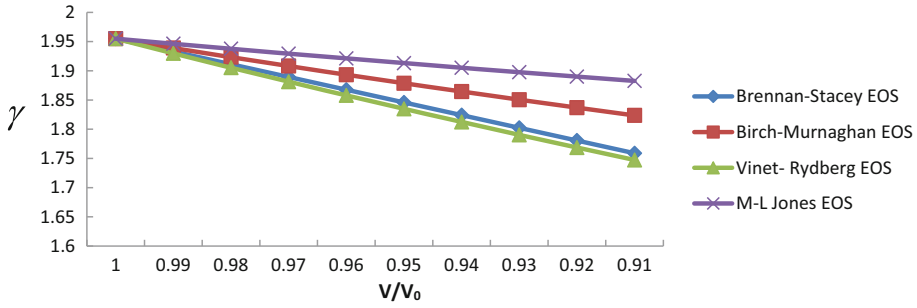

Fig. 1 Gruneisen parameter of $Fe_{12}Cr_{12}W_4C_{12}$ at high compressions

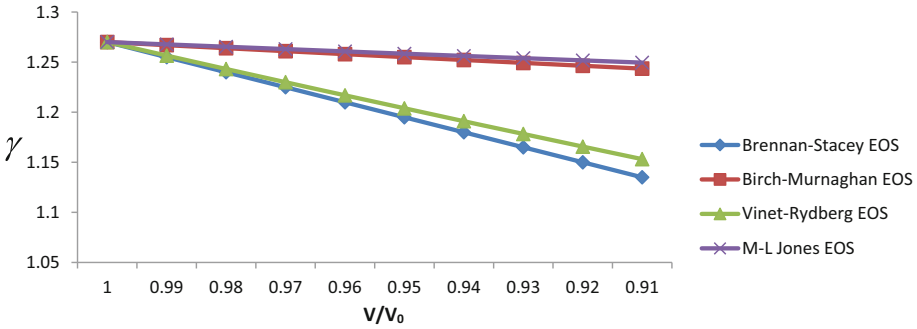

Fig. 2 Gruneisen parameter of Fe_2B at high compressions

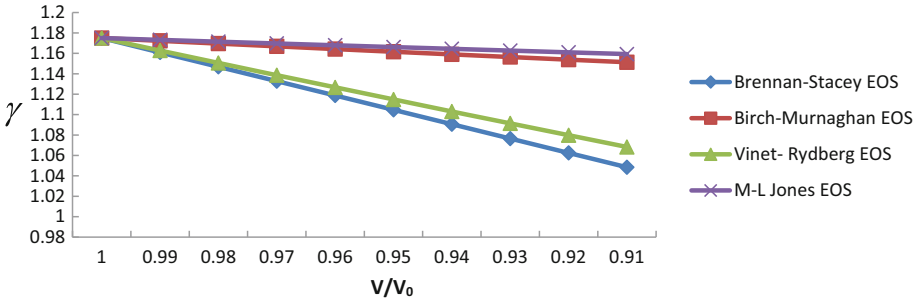

Fig. 3 Gruneisen parameter of Fe_3C at high compressions

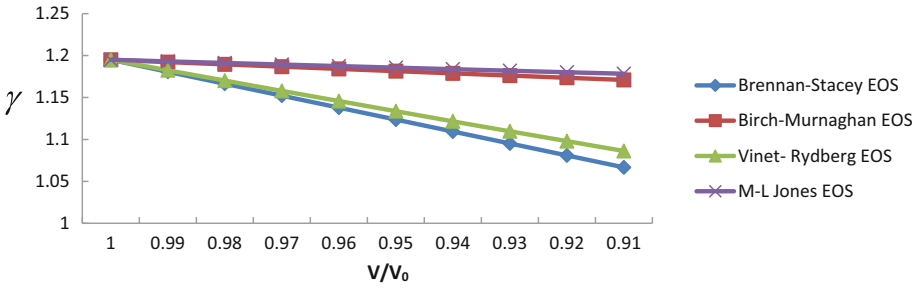

Fig. 4 Gruneisen parameter of $Fe_{12}Cr_{12}W_4C_8B_4$ at high compressions

using Eq. (4), as shown in Fig. 2 and Table 2. Particularly, the modified Lenard Jones EOS displays a minimal slope, while the Brennan–Stacey EOS having the maximum slope. This observation is consistent with the graphical representation and numerical data. By applying Eq. (4) to determine the slope of the plots, it becomes evident that the graph depicting the Gruneisen parameter derived from the modified Lenard Jones EOS forms an angle of 12.80 with respect to the (V/V_0) axis. Conversely, the Brennan–Stacey EOS graph forms an angle of 56°. Such findings underscore the notable difference in behavior, indicating that values obtained from the modified Lenard Jones EOS remain relatively constant at higher compression levels in comparison with other models. Further analysis employing the Birch–Murnaghan EOS demonstrates that the Gruneisen parameter graph derived from this equation forms an angle of 16.30. This suggests that the Birch–Murnaghan EOS and the modified Lenard Jones EOS perform similarly in predicting the Gruneisen parameter up to a compression range of 0.95. However, as compression increases beyond this

Table 2 Calculation of Pressure and Gruneisen parameter at high compression for Fe_2B

V/V_0	Pressure(GPa)				Gruneisen parameter			
	Brennan–Stacey EOS	Birch–Murnaghan EOS	Vinet–Rydberg EOS	M-L Jones EOS	Brennan–Stacey EOS	Birch–Murnaghan EOS	Vinet–Rydberg EOS	M-L Jones EOS
1	0	0	0	0	1.27	1.27	1.27	1.27
0.99	3.402016	3.402153	3.402033	3.402161	1.254971	1.266946	1.256512	1.26765
0.98	6.993734	6.994878	6.993882	6.994945	1.239951	1.26392	1.243162	1.265317
0.97	10.78528	10.7893	10.78581	10.78953	1.224938	1.260922	1.229943	1.263003
0.96	14.78735	14.79727	14.78868	14.79785	1.209932	1.257952	1.216852	1.260707
0.95	19.01128	19.03146	19.01403	19.03264	1.194933	1.255009	1.203883	1.258429
0.94	23.46905	23.50539	23.4741	23.5075	1.17994	1.252094	1.191031	1.256169
0.93	28.17335	28.23351	28.18187	28.23699	1.164952	1.249206	1.178292	1.253926
0.92	33.13763	33.23127	33.15112	33.23665	1.149968	1.246346	1.165659	1.251702
0.91	38.37613	38.5152	38.39649	38.52316	1.134989	1.243513	1.15313	1.249495

Table 3 Calculation of pressure and Gruneisen parameter at high compression for Fe_3C

V/V_0	Pressure(GPa)				Gruneisen parameter			
	Brennan–Stacey EOS	Birch–Murnaghan EOS	Vinet–Rydberg EOS	M-L Jones EOS	Brennan–Stacey EOS	Birch–Murnaghan EOS	Vinet–Rydberg EOS	M-L Jones EOS
1	0	0	0	0	1.175	1.175	1.175	1.175
0.99	2.661193	2.661295	2.66121	2.661304	1.16092	1.172282	1.162767	1.173214
0.98	5.465516	5.466363	5.465653	5.466432	1.146846	1.169585	1.150637	1.171438
0.97	8.420377	8.42335	8.420866	8.423593	1.132778	1.166909	1.138607	1.169672
0.96	11.53361	11.54093	11.53483	11.54153	1.118715	1.164256	1.126672	1.167917
0.95	14.81347	14.82836	14.81598	14.82957	1.104656	1.161623	1.114829	1.166172
0.94	18.26873	18.29548	18.27329	18.29765	1.090602	1.159012	1.103073	1.164438
0.93	21.90861	21.95283	21.91624	21.95641	1.07655	1.156423	1.091402	1.162714
0.92	25.74291	25.81163	25.7549	25.81717	1.062501	1.153855	1.07981	1.161001
0.91	29.78197	29.88388	29.79995	29.89206	1.048455	1.151308	1.068295	1.159298

Table 4 Calculation of pressure and Gruneisen parameter at high compression for $Fe_{12}Cr_{12}W_4C_{12}$

V/V_0	Pressure(GPa)				Gruneisen parameter			
	Brennan–Stacey EOS	Birch–Murnaghan EOS	Vinet–Rydberg EOS	M-L Jones EOS	Brennan–Stacey EOS	Birch–Murnaghan EOS	Vinet–Rydberg EOS	M-L Jones EOS
1	0	0	0	0	1.955	1.955	1.955	1.955
0.99	3.710306	3.710379	3.710264	3.710471	1.933129	1.938999	1.929891	1.946265
0.98	7.680844	7.681464	7.680502	7.682231	1.911282	1.923379	1.90535	1.937714
0.97	11.92866	11.9309	11.9275	11.9336	1.889457	1.908126	1.881351	1.929343
0.96	16.47197	16.47763	16.46921	16.48433	1.867654	1.893227	1.857866	1.921148
0.95	21.33024	21.34203	21.32481	21.3557	1.845871	1.878669	1.834873	1.913123
0.94	26.52425	26.546	26.51485	26.57072	1.824107	1.864439	1.812347	1.905266
0.93	32.07626	32.11312	32.06131	32.15419	1.802361	1.850525	1.790266	1.897572
0.92	38.01002	38.06876	37.98773	38.13294	1.780632	1.836917	1.768609	1.890037
0.91	44.351	44.44029	44.31932	44.53598	1.758919	1.823604	1.747357	1.882657

Table 5 Calculation of pressure and Gruneisen parameter at high compression for $Fe_{12}Cr_{12}W_4C_8B_4$

V/V_0	Pressure(GPa)				Gruneisen parameter			
	Brennan–Stacey EOS	Birch–Murnaghan EOS	Vinet–Rydberg EOS	M-L Jones EOS	Brennan–Stacey EOS	Birch–Murnaghan EOS	Vinet–Rydberg EOS	M-L Jones EOS
1	0	0	0	0	1.195	1.195	1.195	1.195
0.99	3.14889	3.149012	3.148909	3.149022	1.18072	1.192241	1.18251	1.193101
0.98	6.468449	6.469466	6.468607	6.469542	1.166447	1.189505	1.17013	1.191215
0.97	9.96757	9.97114	9.968133	9.971405	1.15218	1.186792	1.157856	1.18934
0.96	13.65565	13.66445	13.65705	13.6651	1.137919	1.184101	1.145684	1.187477
0.95	17.54262	17.5605	17.54551	17.56182	1.123662	1.181434	1.13361	1.185625
0.94	21.63898	21.67114	21.64425	21.67351	1.10941	1.178789	1.121629	1.183786
0.93	25.95584	26.00901	25.96466	26.01291	1.095161	1.176167	1.109737	1.181958
0.92	30.50495	30.58761	30.51884	30.59366	1.080916	1.173568	1.097932	1.180143
0.91	35.29876	35.42136	35.3196	35.43031	1.066672	1.170991	1.086208	1.178339

point, the modified Lenard Jones EOS emerges as the more reliable model for accurately predicting the behavior of Fe2B at higher compression ratios.

$$\text{Slope}\ \frac{d\gamma}{d\left(\frac{V}{V_0}\right)} = \left[\frac{\gamma_2-\gamma_1}{\left(\frac{V}{V_0}\right)_2-\left(\frac{V}{V_0}\right)_1}\right].$$

So the slope for modified Lenard Jones EOS is

$$\left[\frac{d\gamma}{d\left(\frac{V}{V_0}\right)}\right]_{M-L\ \ \text{Jones}} = \frac{1.159798-1.175}{0.91-1} = 0.16891.$$

and the slope for Brennan–Stacey EOS is

$$\left[\frac{d\gamma}{d\left(\frac{V}{V_0}\right)}\right]_{\text{Brennan}-\text{StaceyEOS}} = \frac{1.048555-1.175}{0.91-1} = 1.40.$$

By analyzing Fig. 3 and Table 3, it is apparent that the modified Lenard Jones EOS has the least slope, while the Brennan–Stacey EOS exhibits the highest slope. The slope calculations, derived from Eq. (4), reveal that the Gruneisen parameter graph derived from the modified Lenard Jones EOS forms an angle of 9.50 degrees with the (V/V_0) axis. Further, the Brennan–Stacey EOS graph creates an angle of 54.460 degrees with the same axis. These observations suggest that the values obtained from the modified Lenard Jones EOS remain relatively constant at higher compression levels compared to others. Further calculations for the Birch–Murnaghan EOS show that its Gruneisen parameter graph forms an angle of 14.70 degrees. This indicates that, up to a compression ratio of 0.95, both the Birch–Murnaghan EOS and the modified Lenard Jones EOS are equally effective in calculating the Gruneisen parameter. However, at higher compression ratios, the modified Lenard Jones EOS emerges as the superior choice among all EOSs for Fe3C, offering more accuracy and stability.

$$\text{Slope}\ \frac{d\gamma}{d\left(\frac{V}{V_0}\right)} = \left[\frac{\gamma_2-\gamma_1}{\left(\frac{V}{V_0}\right)_2-\left(\frac{V}{V_0}\right)_1}\right].$$

So the slope for modified Lenard Jones EOS is

$$\left[\frac{d\gamma}{d\left(\frac{V}{V_0}\right)}\right]_{M-L\ \ \text{Jones}} = \frac{1.178339-1.195}{0.91-1} = 0.18512.$$

and the slope for Brennan–Stacey EOS is

$$\left[\frac{d\gamma}{d\left(\frac{V}{V_0}\right)}\right]_{\text{Brennan}-\text{StaceyEOS}} = \frac{1.066672-1.195}{0.91-1} = 1.42586.$$

Based on Fig. 4 and Table 5, it is evident that the modified Lenard Jones equations of states (EOS) demonstrates the lowest slope, while the Brennan–Stacey EOS exhibits the highest slope. Using Eq. (4) for slope calculations of the plots, we can observe that the graph derived from the modified Lenard Jones EOS forms an angle of 10.470 degrees with the (V/V_0) axis, whereas the Brennan–Stacey EOS forms an angle of 54.950 degrees. These calculations highlight that the values obtained from the modified Lenard Jones EOS remain relatively constant at higher compression levels compared to others. Similarly, upon analyzing the Birch–Murnaghan EOS, the Gruneisen parameter obtained forms an angle of 14.890 degrees. The whole story indicates that the Birch–Murnaghan EOS and the modified Lenard Jones EOS are equally effective in calculating the Gruneisen parameter up to a compression ratio of 0.95. However, as we move compression ratios, the modified Lenard Jones EOS seems as the very best choice among the EOSs considered for $Fe_{12}Cr_{12}W_4C_8B_4$ due to its consistency and reliability.

4 Conclusions

Based on the provided results and observations, we can draw the following conclusions: Comparison of EOS Angles: The Gruneisen parameter graph obtained from the modified Lenard Jones EOS makes an angle of approximately 38.790, 12.80, 9.50, and 10.470 with the (V/V_0) axis for different materials ($Fe_{12}Cr_{12}W_4C_{12}$, Fe_2B, Fe_3C, and $Fe_{12}Cr_{12}W_4C_8B_4$, respectively). The Vinet–Rydberg EOS graph forms an angle of approximately 660 for $Fe_{12}Cr_{12}W_4C_{12}$. The Brennan–Stacey EOS graphs form angles of approximately 560, 54.460, and 54.950 for $Fe_{12}Cr_{12}W_4C_{12}$, Fe_2B, and $Fe_{12}Cr_{12}W_4C_8B_4$, respectively. The Birch–Murnaghan EOS graph forms angles of approximately 16.30, 14.70, and 14.890 for $Fe_{12}Cr_{12}W_4C_{12}$, Fe_2B, and $Fe_{12}Cr_{12}W_4C_8B_4$, respectively.

4.1 Behavior of Modified Lenard Jones EOS

The values obtained from the modified Lenard Jones EOS exhibit a trend of decreasing, but very slowly, as the compression increases. This is observed for different materials. The modified Lenard Jones EOS values remain almost constant at high compression levels in comparison with other EOS models (Brennan–Stacey and Birch–Murnaghan).

4.2 EOS Suitability for Gruneisen Parameter Calculation

The modified Lenard Jones EOS is stated to be useful for calculating the Gruneisen parameter up to a compression range of 0.91 for $Fe_{12}Cr_{12}W_4C_{12}$, 0.95 for Fe_2B, and 0.95 for Fe_3C. At higher compression ratios, the modified Lenard Jones EOS is suggested to be the best overall EOS for calculating the Gruneisen parameter for Fe_2B, Fe_3C and $Fe_{12}Cr_{12}W_4C_8B_4$.

4.3 Birch–Murnaghan EOS Comparison

The Birch–Murnaghan EOS is noted to be equally useful as the modified Lenard Jones EOS in calculating the Gruneisen parameter up to a compression range of 0.95 for different materials.

4.4 High Compression Behavior

The modified Lenard Jones EOS values are observed to be almost constant at high compression, making it potentially more suitable for these conditions compared to other EOS models. In summary, the modified Lenard Jones EOS exhibits specific advantages in terms of its behavior at high compressions and its suitability for calculating the Gruneisen parameter for various materials. However, the Birch–Murnaghan EOS also performs well in certain cases. The specific choice of EOS model would depend on the material being studied and the compression range of interest (Srivastava et al. 2023d, e).

Acknowledgements Not applicable

Authors Contributions All the authors have write and reviewed whole manuscript. Dr. Anjani Kumar Pandey have made Figures and Dr. Chandra Kumar Dixit have given idea to write the manuscript. Dr. Chandra Kumar Dixit have supervised the research and equally contributed as first author.

Funding The authors declare that they have no funding agency available.

Data Availability Not applicable.

Declarations

Conflicts of interests The authors affirm that they possess no discernible conflicting financial interests or personal affiliations that could have potentially influenced the findings presented in this manuscript.

Ethical Approval The authors assure that the manuscript is authors own work which has not been previously published elsewhere.

Consent to Participate Not applicable.

Consent for Publication Not applicable.

Declaration of generative AI and AI-assisted technologies in the writing process During the preparation of this work the author(s) used ChatGpt in order to improve language. After using this tool/service, the author(s) reviewed and edited the content as needed and take(s) full responsibility for the content of the publication.

References

Barton MA, Stacey FD (1985) The Grüneisen parameter at high pressure: a molecular dynamical study. Phys Earth Planet Interior 39:167

Birch F (1947) Finite elastic strain of cubic crystals. Phys Rev 71:809

Dixit CK, Srivastava S, Singh P, Pandey AK (2024) Analysis of finite strain theory for modeling a new EOS for nanomaterials. Nano-Struct Nano-Objects 38:101121

Feng J, Xiao B, Zhou R, Jiang YH, Cen QH (2012) Calculation and simulation for the mechanical properties of carbides and borides in cast iron. Proc Eng 31:676

Jang JH, Kim IG, Bhadeshi HKDH (2009) Substitutional solution of silicon in cementite: a first-principles study. Comput Mater Sci 44:1319

Moustafa IM, Moustafa MA, Nofal AA (2000) Carbide formation mechanism during solidification and annealing of 17% Cr-ferritic steel. Mater Lett 42:371

Music D, Kreissig U, Mertens R, Schneider JM (2004) Electronic structure and mechanical properties of Cr7C3. Phys Lett A 326:473

Pandey AK, Srivastava S, Dixit CK et al (2023a) Shape and size dependent thermophysical properties of nanomaterials. Iran J Sci 47:1861–1875

Pandey A, Srivastava S, Dixit CK (2023b) A paradigm shift in high-pressure equation of state modeling: unveiling the pressure-bulk modulus relationship. Iran J Sci 47:1877–1882

Pandey AK, Dixit CK, Srivastava S, Singh P, Tripathi S (2023d) Theoretical prediction of thermo-elastic properties of TiO_2 (Rutile Phase). Natl Acad Sci Lett 8:1–4

Pandey AK, Dixit CK, Srivastava S (2023e) Theoretical model for the prediction of lattice energy of diatomic metal halides. J Math Chem 62:269–274

AK Pandey, S Srivastava, P Singh, S Tripathi, CK Dixit (2023) Theoretical prediction of Grüneisen parameter for nano Lead Sulfide at different compressions. https://doi.org/10.21203/rs.3.rs-3159558/v1

Shein IR, Medvedeva NI, Ivanovskii AL (2006) Electronic and structural properties of cementite-type M3X (M= Fe, Co, Ni; X= C or B) by first principles calculation. Physica B 371:126

Slater JC (1939) Introduction to chemical physics, 1st edn. McGraw Hill Book Co., Newyork

Srivastava S, Pandey AK, Dixit CK (2023a) Theoretical prediction of Grüneisen parameter for γ-Fe_2O_3. Comput Condens Matter 35:e00801

Srivastava S et al (2023b) Equation of states at extreme compression ranges: pressure and Bulk modulus as an example. Materials Open. https://doi.org/10.1142/S2811086223500073

Srivastava S, Pandey AK, Dixit CK (2023c) Theoretical prediction for thermoelastic properties of carbon nanotubes (CNTs) at different pressure or compression using equation of states. J Math Chem 61:2098–2104

Srivastava S, Singh P, Pandey AK, Dixit CK (2023d) Melting temperature of semiconducting nanomaterials at different shape and size. Nano-Struct Nano-Objects 36:101067

Srivastava S, Pandey AK, Dixit CK (2023e) Comparative study of elastic properties of some inorganic and organic molecular crystals from EOS. J Math Chem. https://doi.org/10.1007/s10910-023-01546-9

Srivastava S, Singh P, Pandey AK, Dixit CK (2023f) Theoretical prediction for thermo elastic properties of nano CdSe (rock salt phase). In: AIJR proceedings, pp 1–5. https://doi.org/10.21467/proceedings.161.1

Srivastava S, Dixit CK, Pandey AK (2023g) Comparative study of elastic properties of some inorganic and organic molecular crystals by using isothermal EOS Available at SSRN: http://ssrn.com/abstract=4427891 or https://doi.org/10.2139/ssrn.4427891

Srivastava S, Singh P, Pandey A, Dixit CK (2024) Unified EOS incorporating the finite strain theory for explaining thermo elastic properties of high temperature superconductors, nanomaterials and bulk metallic glasses. Solid State Commun 377:115387

Stacey FD, Brennan BJ, Irvine RD (1981) Geophys Surv 4:189

Sun J (2005) A modified Lennard-Jone-Type equation of state for solids strisfying the spinodal condition. J Phys: Condens Matter 17(12):L103–L111

Uhlenhaut DI, Kradolfer J, Püttgen W, Löffler JF, Uggowitzer PJ (2006) Structure and properties of a hypoeutectic chromium steel processed in the semi-solid state. Acta Mater 54:2727

Vinet P, Ferrante J, Smith JR, Rose JH (1986) Compressibility of solids. J Phys C 92:L467

Xiao B, Feng J, Zhou CT, Xing JD, Xie XJ, Cheng YH, Zhou R (2010) The elasticity, bond hardness and thermodynamic properties of X2B (X=Cr, Mn, Fe, Co, Ni, Mo, W) investigated by DFT theory. Phys b: Condens Matter 405(5):1274–1278

Xiao B, Feng J, Zhou CT, Jiang YH, Zhou R (2011) Mechanical properties and chemical bonding characteristics of Cr7C3 type multicomponent carbides. J Appl Phys 109:023507

Xie JY, Chen NX, Shen J, Teng LD, Seetharaman S (2005) Atomistic study on the structure and thermodynamic properties of Cr7C3, Mn7C3, Fe7C3. Acta Mater 53:2727

Zhou CT, Xiao B, Feng J, Xing JD, Xie XJ, Chen YH, Zhou R (2009a) First principles study on the elastic properties and electronic structures of (Fe, Cr) 3C. Comput Mater Sci 45:986

Zhou CT, Xing JD, Xiao B, Feng J, Xie XJ, Chen YH (2009b) First principles study on the structural properties and electronic structure of X2B (X= Cr, Mn, Fe, Co, Ni, Mo and W) compounds. Comput Mater Sci 44:1056

Zuo Y-T, Liu H-J (2021) Fractal approach to mechanical and electrical properties of graphene/sic composites. Facta Univ-Series Mech Eng 19(2):271–284